Cryogenic Toughness of Commercial Aluminum-Lithium Alloys: Role of Delamination Toughening

K.T. VENKATESWARA RAO, WEIKANG YU, and R.O. RITCHIE

Mechanisms influencing the plane-strain fracture toughness behavior of commercial aluminum-lithium alloys at cryogenic temperatures are investigated as a function of microstructure and plate orientation. It is confirmed that certain alloys show a marked *increase* in tensile ductility and toughness with *decrease* in temperature, although such behavior is not found in the short-transverse orientations, nor for all alloys and aging conditions. Specifically at lower temperatures, the majority of Al-Li alloys, namely 2090-T8E41, 8091-T8X, 8090-T8X, and 2091-T351, show a significant *increase* in fracture toughness in the in-plane orientations (L-T,T-L), without any apparent change in fracture mode. Such behavior is attributed primarily to loss of through-thickness constraint resulting from enhanced short-transverse delamination (termed crack-divider delamination toughening), consistent with observed reductions in plane-strain ductility and short-transverse (S-L,S-T) toughness. Conversely, in underaged microstructures of 8091, 8090, and peak-aged 2091, a decrease in toughness with decreasing temperature is found for both L-T and S-L orientations, behavior which is associated conversely with a fracture-mode change from ductile void coalescence to brittle transgranular shear and intergranular delamination at lower temperatures.

I. INTRODUCTION

THE rapid development of advanced aluminum-lithium alloys in recent years has been driven largely by numerous potential structural applications in the aerospace industry requiring high-strength, high-modulus, and low-density metallic materials. More recently, however, there has been increasing interest in the cryogenic properties of these alloys, following reports of a marked *increase* in ductility, fatigue resistance, and especially fracture toughness with *decrease* in temperature from ambient to 4 K.[1-5] Thus, although developed primarily as low-density high-strength airframe materials, Al-Li alloys have additionally become attractive candidate materials for liquid-hydrogen, -oxygen, and -natural gas fuel tanks, in particular for existing and future transatmospheric and hypersonic aircraft applications.

The mechanistic origin of the significantly improved cryogenic properties of aluminum-lithium alloys currently is uncertain, although behavior is not unlike other high-strength aluminum alloys (*e.g.*, 2219) which display somewhat higher K_{Ic} values at lower temperatures.[6] Explanations based on higher strain-hardening rates, associated with more homogeneous plastic deformation,[7,8] and solidification of Na, K, H-rich liquid phases at grain boundaries[2,3,9] have been proposed for Al-Li alloys, although such suggestions seemingly are inconsistent with results[4,10] which show *increased* low-temperature fracture toughness for the longitudinal (L-T,T-L) orientations but *decreased* toughness for the short-transverse (S-L,S-T) orientations. The latter observations led to proposals[4,10] that the effect was associated more with a greater tendency for short-transverse cracking along high angle grain boundaries at low temperatures, similar to the early work of Carman *et al.*[11] on the toughness of 7075-T6. Such increased short-transverse cracking leads to enhanced crack deflection[10] and, more importantly, to delamination perpendicular to the crack plane[4,10] for fracture in the L-T and T-S orientations, as illustrated for the crack-divider and crack-arrester orientations, respectively, in Figure 1.

Since extensive low-temperature fracture-toughness data on commercial aluminum-lithium alloys are not readily available in the literature, the prime objective of the present study is to examine whether the excellent cryogenic deformation and toughness properties reported for 2090-T8E41[1,7,10] are common to other Al-Li alloys. Moreover, as grain structures in these materials vary in their degree of coarseness, recrystallization, and texture, all factors which may markedly affect the extent of short-transverse cracking, the intent is to study the temperature-dependence of the toughness as a function of microstructure and plate orientation in order to evaluate the mechanisms of toughening resulting from delamination perpendicular to crack plane.

II. EXPERIMENTAL PROCEDURES

A. *Materials and Microstructures*

Commercial 11 to 16 mm thick plates of aluminum-lithium alloys 2090, 2091, 8090, and 8091, of composition shown in Table I, were studied in the naturally-aged T351 (underaged) and peak-aged T8X conditions; heat treatments are summarized in Table II.

Microstructural characterization, performed using optical and transmission electron microscopy, revealed a wide range of precipitates, as summarized in Table III and discussed in detail elsewhere.[12-16] All alloys showed

K.T. VENKATESWARA RAO is a Postdoctoral Research Engineer, and R.O. RITCHIE is a Professor and the Director of the Center for Advanced Materials, Materials and Chemical Sciences Division, Lawrence Berkeley Laboratory, and Department of Materials Science and Mineral Engineering, University of California, Berkeley, CA 94720. WEIKANG YU, formerly with the Department of Materials Science and Mineral Engineering, University of California, Berkeley, is with Raychen Corporation, Menlo Park, CA.

Manuscript submitted April 1, 1988.

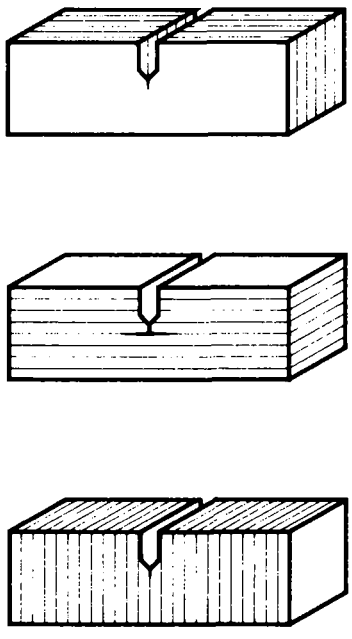

Fig. 1—Terminology used to describe the various orientations for crack extension in an anisotropic material containing specific planes of weakness in one direction. Note that the L-T and T-L orientations correspond to crack divider, T-S and L-S to crack arrester, and S-L and S-T to crack delamination (or short-transverse).

a highly anisotropic grain structure (*e.g.*, Figure 2), with pancake-shaped grains elongated in the rolling direction; grain sizes were fairly coarse, typically 500 μm wide by 50 μm thick by several millimeters long, except in 8091 where they were considerably smaller. All structures were unrecrystallized, except in 2091 where some degree of recrystallization was evident. Strong deformation textures are seen in all alloys due to prior cold working processes; these textures have been found to be predominantly of the brass type ($\{110\}\langle 112\rangle$) with evidence of weaker S ($\{123\}\langle 634\rangle$) and copper ($\{112\}\langle 111\rangle$) types.[17,18,19]

The alloys were strengthened by very fine, homogeneous, matrix distributions of coherent, ordered, spherical δ' (Al_3Li) precipitates and β' (Al_3Zr) dispersoids in the underaged T351 tempers. On aging to a peak-aged T8 condition, coarsening of δ' precipitates was apparent, together with the matrix precipitation of T_1 (Al_2CuLi) and θ'-like (Al_2Cu/Al_2CuLi) plates in 2090 (Figures 3(a) and (b)). Also evident was fine precipitation of T_1 plates along subgrain boundaries with narrow δ'-precipitate-free-zones (PFZs) of less than ~100 nm in width. In the Mg-containing alloys (except 2091), T_1 and θ' plates were replaced by S (Al_2CuMg) or S′ (precursor to S) laths in the matrix (Figure 3(c)). In 8090-T8X, this resulted in a small degree of precipitation along high-angle grain boundaries and the consequent formation of small (~500 nm) δ'-PFZs; in 8091-T8X, grain-boundary precipitation was more extensive and PFZs were correspondingly wider (~1 μm) (Figure 3(d)). Conversely, in 2091, artificial aging only coarsened the δ'-precipitates in the matrix without any evidence of S′ or T_1 precipitates.

B. *Mechanical Properties*

Fracture-toughness testing was performed in accordance with ASTM Standard E 399-83* with 6 to 8 mm thick compact C(T) and single-edged-notched bend SEN(B) samples loaded in four-point bending, for the L-T and T-S orientations and double-cantilever-beam (DCB) specimens for the S-L orientation. All specimens were initially fatigue precracked, at a load ratio ($R = K_{min}/K_{max}$) of 0.1, to a crack length-to-specimen width ratio (a/W) of 0.45 to 0.55, and tested at both ambient (298 K) and liquid-nitrogen (77 K) temperatures. All results represent plane-strain values, except where noted. Corresponding uniaxial tensile properties (longitudinal L direction) were assessed using 6.4-mm-round tensile specimens with a 25 mm gage length. Ambient-temperature mechanical properties are included in Table IV.

*Although not specified in the Standard, due to the limited plate thickness, it was necessary to use DCB specimens for all short-transverse tests.

Fatigue-precracked compact C(T) specimens of 2090-T8E41, with varying thickness between 0.5 and 13 mm, were used to study the influence of thickness on fracture toughness; anti-buckling guides were employed to prevent out-of-plane shear in the thinner geometries. Since the through-thickness strength variations of commercial Al-Li alloy plate can be as large as 20 pct,[17] all specimens were machined from the plate midsection.

Additional tests were performed at 298 and 77 K on circumferentially-notched tensile samples, with notch-root radii, ρ, varying between 0.6 and 3.2 mm, to evaluate the influence of stress state on ductility.[20] Strains were monitored continuously at the diameter at the notch root using a diametral extensometer; fracture strains were measured from the average cross-section at failure and computed from the Bridgman analysis as[21]

$$\bar{\varepsilon}_p = 2 \ln\left(\frac{r_0}{r_{min}}\right) \qquad [1]$$

where $\bar{\varepsilon}_p$ is the equivalent plastic strain and r_0 and r_{min} are the initial and minimum radii of the notched cross-section. With this geometry, the stress-state at the center of the specimen, defined in terms of the ratio of hydrostatic stress, σ, to equivalent stress, $\bar{\sigma}$, is given by

Table I. Nominal Chemical Compositions of Commercial Aluminum-Lithium Alloys Investigated (Wt Pct)

		Li	Cu	Mg	Zn	Fe	Si	Ti	Zr	Al
Alcoa	2090	2.05	2.86	0.01	0.005	0.02	0.01	0.02	0.12	bal
Pechiney	2091	1.7 to 2.3	1.8 to 2.5	1.1 to 1.9	0.25	0.3	0.2	0.1	0.04 to 0.16	bal
Alcan	8090	2.50	1.30	0.70	—	0.2	0.1	—	0.12	bal
Alcan	8091	2.60	1.90	0.90	—	0.1	0.1	—	0.12	bal

Table II. Heat Treatments Utilized on Commercial Alloys

Alloy	Condition	Heat Treatment
2090	T8E41 (peak aged)	solution treat, 6 pct stretch, aged 24 h at 163 °C
	OA (overaged)	T8E41 + 1000 h at 163 °C
2091	T351 (underaged)	solution treat, 3 pct stretch, naturally aged*
	T8X (peak aged)	solution treat, 3 pct stretch, aged 10 h at 135 °C
8090	T351 (underaged)	solution treat, 3 pct stretch, naturally aged*
	T8X (peak aged)	solution treat, 3 pct stretch, aged 16 h at 190 °C
8091	T351 (underaged)	solution treat, 3 pct stretch, naturally aged*
	T8X (peak aged)	solution treat, 3 pct stretch, aged 16 h at 190 °C

*Tested in stable condition approximately six months after solution treatment and stretching.

$$\sigma/\bar{\sigma} = \frac{1}{3} + \ln\left(1 + \frac{r_{\min}}{2\rho}\right) \quad [2]$$

C. *Fractography*

Scanning electron microscopy (SEM) was performed on all fractured samples to elucidate the failure mechanisms. In addition, metallographic sections were taken of the crack-path morphology, both parallel and perpendicular to the crack-growth direction. Parallel sections were taken at the specimen mid-thickness, with the cracks impregnated with epoxy for better edge retention.

III. RESULTS

A. *Uniaxial Tensile Properties*

Uniaxial tensile properties of the commercial Al-Li alloys at 77 and 298 K are compared in Table IV. Yield and tensile strengths show a ~10 to 40 pct increase at 77 K; surprisingly, elongation values show a larger increase by ~10 to 75 pct and strain-hardening coefficients by a factor of approximately two. Thus, in the L direction examined, strength, ductility, and strain-hardening rates all *increase* with *decrease* in temperature. All tensile failures at 77 K were seen to occur at maximum load, without evidence of any necking prior to fracture.

B. *Fracture-Toughness Properties*

Plane-strain fracture-toughness data also are listed in Table IV. It can be seen that, at both low and high temperatures, K_{Ic} values for the L-T (crack-divider) orientation exceed those for the S-L (crack-delamination) orientation by between 18 and 375 pct; additional results in 2090-T8E41 show that the toughness in the T-S (crack-arrester) orientation exceeds that in the L-T orientation by 80 pct. However, the low-temperature strength-toughness properties of all Al-Li alloys in the L-T orientation, except 8090-T351 and 8091-T351, are superior to those of traditional high-strength aluminum alloys[22] (Figure 4). However, not all alloys show increasing toughness with decreasing temperature. As illustrated in Figure 5, compared to ambient-temperature behavior, only 2090-T8E41, 2091-T351, 8090-T8X, and 8091-T8X have higher K_{Ic} values at 77 K in the L-T orientation; conversely, 2091-T8X, 8090-T351, and 8091-T351 display the more common behavior of lower toughness values at the lower temperature. However, all alloys show a small decrease in toughness with decreasing temperature for the short-transverse (S-T) orientation.*

*It should be noted that data points were obtained only at 77 and 298 K, except in 2090. However, studies on 8090[51] also have shown similar monotonic trends over this temperature range.

C. *Fractography*

A distinction between alloys which show increasing rather than decreasing toughness at lower temperatures is evident from observations of fracture-surface and crack-path morphology. Illustrated in Figure 6 are the fracture surfaces for 2091-T8X at 298 and 77 K in the L-T (crack-divider) orientation. Clearly apparent is a change from ductile fracture (microvoid coalescence around cracked

Table III. Summary of the Grain-Size Dimensions and Strengthening Precipitates in Aluminum-Lithium Alloys

Alloy	Grain Size			Primary Hardening Precipitates
	L (mm)	T (μm)	S (μm)	
2090-T8E41	2 to 3	500	50	$\delta'(Al_3Li)$, $T_1(Al_2CuLi)$, $\theta'(Al_2Cu)$, $\beta'(Al_3Zr)$
2091-T351	1 to 2	600	40	$\delta'(Al_3Li)$, $\beta'(Al_3Zr)$
2091-T8X				$\delta'(Al_3Li)$, $\beta'(Al_3Zr)$
8090-T351	1 to 2	350	40	$\delta'(Al_3Li)$, $\beta'(Al_3Zr)$
8090-T8X				$\delta'(Al_3Li)$, $T_1(Al_2CuLi)$, $S'(Al_2CuMg)$, $\beta'(Al_3Zr)$
8091-T351	0.25	65	25	$\delta'(Al_3Li)$, $\beta'(Al_3Zr)$
8091-T8X				$\delta'(Al_3Li)$, $S'(Al_2CuMg)$, $\beta'(Al_3Zr)$

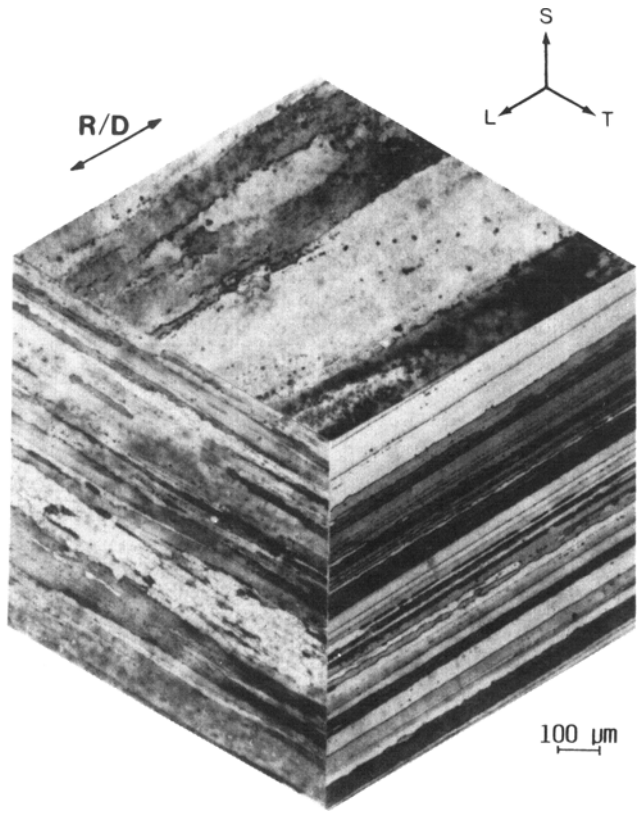

Fig. 2—Typical three-dimensional microstructure of commercial aluminum-lithium alloys, showing unrecrystallized, pancake-shaped grains, elongated along the rolling direction. Optical micrograph obtained for 2090-T8E41 alloy, using Keller's reagent etch.

or uncracked Fe-Cu-rich intermetallics and constituent particles, with large macroscopic shear lips) at 298 K to brittle transgranular shear failure (with intergranular delamination bands or secondary cracks running parallel to the crack-growth direction and normal to the short-transverse direction) at 77 K, a transition which induces a marked change in crack-path morphology (Figures 6(c), (f) and 8(a), (b)). Such behavior is typical of microstructures which have lower fracture toughness (L-T) at cryogenic temperatures, namely 2091-T8X, 8090-T351, and 8091-T351.

Conversely, microstructures which show higher fracture toughness (L-T) at cryogenic temperatures, namely peak-aged 2090, 8090, 8091, and underaged 2091, undergo no such fracture-mode transition over the temperature range 77 to 298 K; a coarse transgranular shear mechanism, with limited regions of void coalescence (around Fe- and Cu-rich intermetallics in 2090) prevails at 77 and 298 K, although the incidence and extent of the intergranular (short-transverse) delamination cracks are markedly enhanced at the lower temperatures (Figure 7). The distinction between these two types of behavior is further exemplified in Figure 8.

Fracture surfaces for the S-L orientation, on the other hand, are totally intergranular for all alloys, and involve a brittle delamination-type failure, decorated with interdispersed 1 to 5 μm diameter Fe-/Cu-rich intermetallic particles,[23] at both high and low temperatures (Figure 9).

IV. DISCUSSION

The present results provide clear confirmation that commercial aluminum-lithium alloys, specifically 2090-T8E41, 2091-T351, 8090-T8X, and 8091-T8X, show a marked improvement in strength, ductility, and (L-T) fracture toughness with decrease in temperature. However, the beneficial low-temperature toughness properties are not seen in the short-transverse orientations and are not apparent at all in certain alloys, namely 2091-T8X, 8090-T351, and 8091-T351, which show a fracture-mode transition from ductile fracture (microvoid coalescence) at 298 K to transgranular-shear mode at 77 K.

These observations, that the temperature dependence of K_{Ic} differs with both orientation and alloy composition/aging condition, would appear to rule out certain published explanations[2,3,7–9] for the increase in toughness with decreasing temperature in Al-Li alloys. For example, Webster[2,3,9] has claimed that the effect is due to the solidification of grain-boundary Na-, K-, and H-rich liquid phases at lower temperatures, an explanation inconsistent with the observed lower short-transverse toughness at 77 K and with the fact that the effect can occur in either underaged or overaged microstructures, depending upon the alloy composition. Explanations based on an increased homogeneity of slip,[7] on the other hand, are consistent with the observed increase in strain-hardening coefficients at lower temperatures, although the higher hardening rates would impart a beneficial influence on fracture toughness only *if the fracture mode is strain-controlled*;[10] however, the explanation is inconsistent with the fact that all alloys/aging conditions show increased strain-hardening coefficients at 77 K, but not all alloys show an increase in K_{Ic}.

In view of the present results, explanations based on the fracture mechanism[4,10] would appear to be far more credible. First, Al-Li alloys, which exhibit a transition with decreasing temperature from ductile tearing (void coalescence) to brittle transgranular shear (with intergranular delamination) (Figures 6 and 8), would be expected to show higher (L-T) K_{Ic} values at 298 K from an increased contribution to the work of fracture from the plastic deformation involved in the tearing process; such behavior[24] has been reported previously for 7075-T6 and 7475-T6 alloys which show such a fracture-mode transition and is generally the expected behavior for the fracture of metals. Conversely, the Al-Li alloys, which have lower (L-T) K_{Ic} values at 298 K, exhibit no apparent change in macroscopic fracture mechanism; the fracture morphology remains brittle transgranular shear at both 77 and 298 K (Figures 7(a) and (b)), similar to reported behavior[6] in 2219-T87 which also shows increasing toughness with decreasing temperature. However, there is clear evidence in these alloys of enhanced short-transverse delamination, perpendicular to the main fracture plane (Figures 7(c) and (f)), at lower temperatures, consistent with the lower low-temperature toughness in the short-transverse orientations.

The intergranular delamination is a result of the poor short-transverse strength, due to the large area fraction of weakened high-angle grain boundaries parallel to the rolling direction. Intergranular precipitation and associated δ'-PFZs, presence of undissolved Fe-Cu-rich

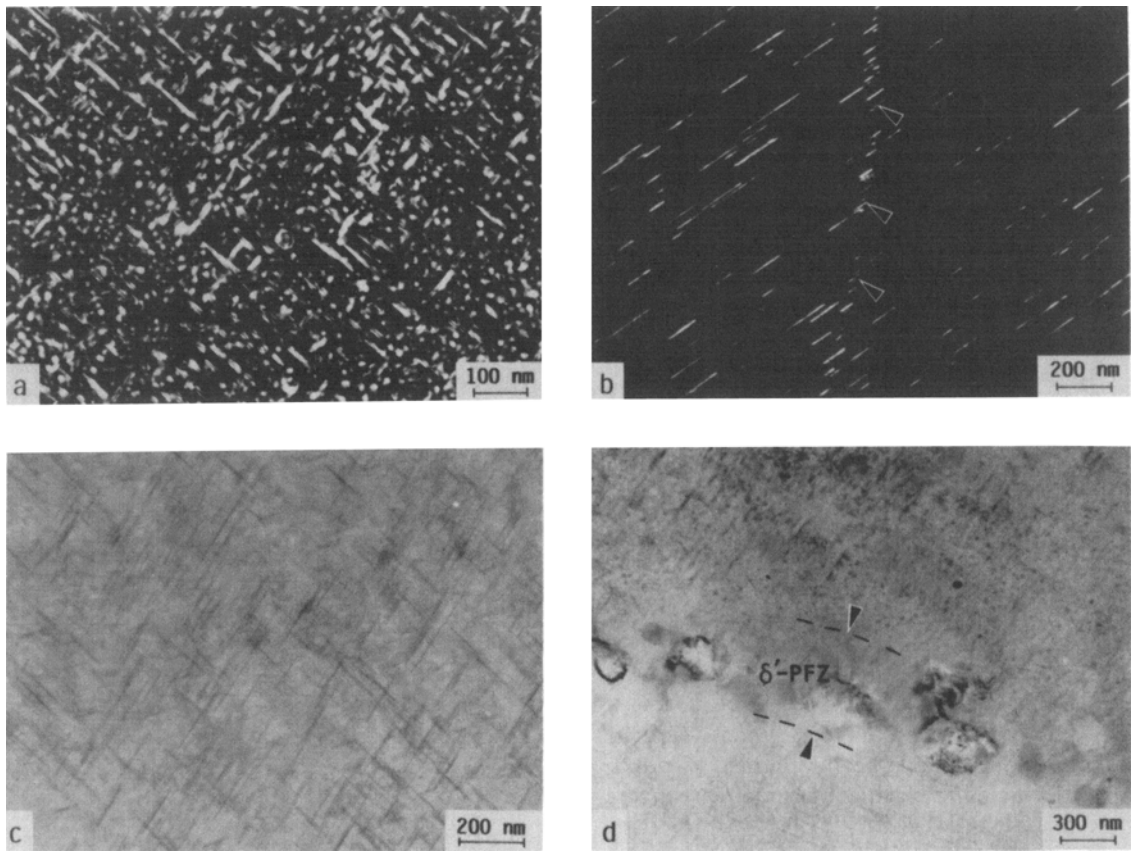

Fig. 3—Transmission electron micrographs of commercial aluminum-lithium alloys showing the prominent microstructural features. Centered dark-field images of (*a*) δ', composite β'-δ', and θ' precipitates; (*b*) T_1 plates in the matrix and along subgrain boundaries (indicated by arrows), in alloy 2090-T8E41; bright-field images (*c*) S' laths; (*d*) δ' PFZs (as shown by arrows) in peak-aged Al-Li-Cu-Mg-Zr alloy 8091 (centered dark-field images in (a) and (b)) were obtained using the δ' and T_1 superlattice reflections, respectively.

Table IV. Fracture Toughness and Tensile Properties* of Commercial Aluminum-Lithium Alloys at 298 and 77 K

	Yield Strength (MPa)		U.T.S. (MPa)		Pct Elongation (on 25 mm)		Fracture Toughness K_{Ic} (MPa$\sqrt{m}$)		Strain-Hardening Exponent (*n*)	
Alloy	298 K	77 K	298 K	77 K	298 K	77 K	298 K	77 K	298 K	77 K
2090-T8E41	552	587	589	642	11	14	36	51† (L-T)	0.06	0.15
							17	15 (S-L)		
							65†	— (T-S)		
2090-OA	466	—	527	—	10	—	22	24 (T-L)		
2091-T351	369	442	451	596	10	16	33†	41† (L-T)	0.12	0.22
							19	17 (S-L)		
2091-T8X	425	483	481	610	8	14	46†	44† (L-T)	0.10	0.21
							25	16 (S-L)		
8090-T351	226	256	352	486	17	24	27†	20 (L-T)	0.19	0.34
							16	17 (S-L)		
8090-T8X	482	—	534	—	6	—	36	38 (L-T)	0.08	—
							13	12 (S-L)		
8091-T351	309	382	417	572	11	14	38†	28 (L-T)	0.16	0.28
							17	10 (S-L)		
8091-T8X	537	574	581	697	6	12	20	38 (L-T)	0.07	0.18
							9	8 (S-L)		

*L direction.
†K_q values not meeting the ASTM plane-strain thickness criterion.

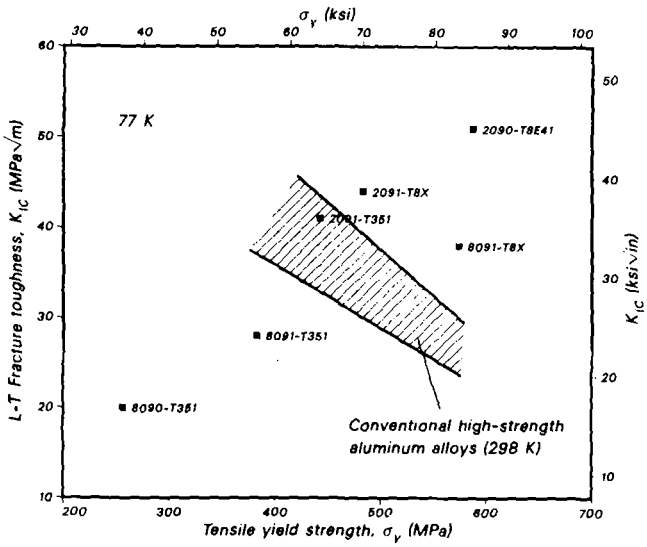

Fig. 4—Combination of yield-strength and fracture-toughness properties for commercial aluminum-lithium alloys at liquid nitrogen temperatures, showing a comparison with ambient temperature data on typical aerospace high-strength aluminum alloys (hatched region after Ref. 22).

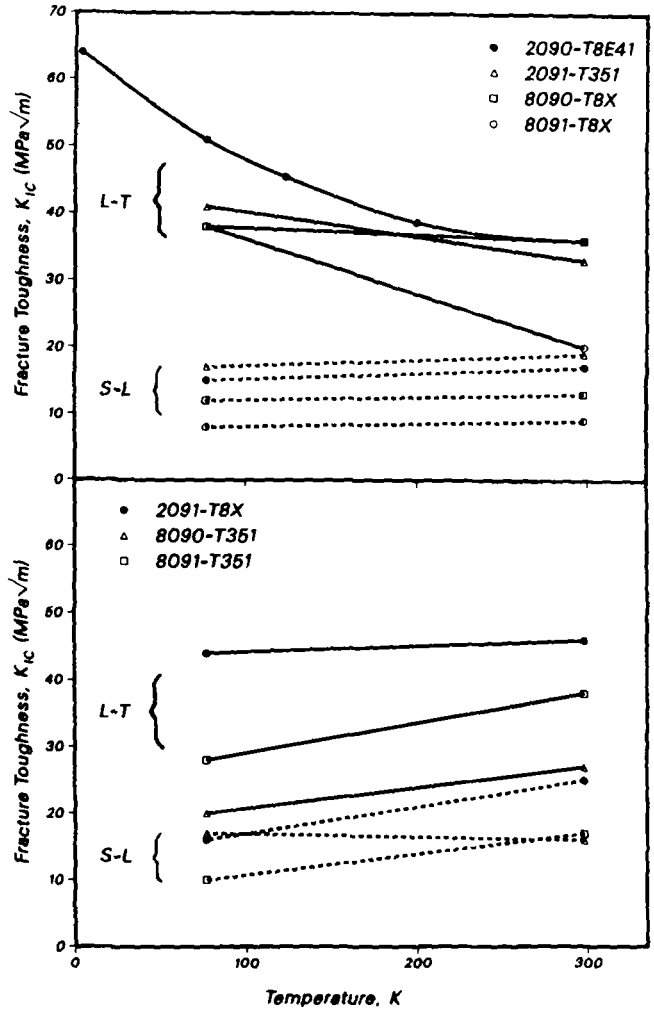

Fig. 5—Variation in fracture toughness K_{Ic} with temperature for commercial aluminum alloys in both L-T and S-L orientations. Note how certain alloys (2090-T8E41, 2091-T351, 8090-T8X, 8091-T8X) show an *increase* in L-T toughness with decreasing temperature, whereas the remainder (2091-T8X, 8090-T351, 8091-T351) show a *decrease*.

intermetallics (Figure 9), and lithium segregation to the grain boundary regions[25] have been identified as prominent reasons influencing the brittle intergranular fracture mode in these materials. Mechanistically, such fractures inevitably are *stress-controlled*,[26] and, therefore, are promoted by factors which elevate the flow stress in the material. In the present alloys, this is achieved at low temperatures by *both* the increase in yield stress *and* the increase in strain hardening exponent.[10]

It is considered that the incidence of such short-transverse delamination is primarily responsible for the improvements in fracture toughness in Al-Li alloys for orientations in the rolling plane (L-T,T-L) at cryogenic temperatures. Similar to behavior in brazed, soldered, or adhesively-bonded multilayer metallic laminates,[27–32] granite rocks,[33] as-deposited substrate-nucleated pyrolytic carbon,[34] and in anisotropic materials where the toughness is low in the short-transverse (S-T,S-L) orientations,[35,36,37] the resulting delamination perpendicular to the crack plane leads to markedly increased fracture toughness in the T-S (crack-arrester) orientations through crack deflection/bifurcation at ~90 deg (the Cook-Gordon mechanism[38] for crack stopping at weak interfaces) as shown for 2090-T8E41 in Figure 10; it also *can* lead to increased toughness in the L-T or T-L (crack-divider) orientations due to loss of through-thickness constraint (Figure 1). In the latter case, toughening is significant only when the through-thickness splitting causes a plane-strain fracture process to be divided in several parallel (thin-sheet) plane-stress fractures with higher K_c values; in high-strength/low toughness materials like pyrolytic carbon,[34] even after through-thickness splitting, the ligaments between the delamination cracks remain in plane strain such that the toughness of the crack-divider orientation is only marginally above that of the short-transverse (presumably, due to the additional work of delamination). However, in aluminum-lithium alloys where plane-strain conditions are mostly met for thicknesses in excess of typically ~5 mm,* crack-divider "delamination toughening" is clearly a reality. In addition, such delamination can increase the degree of in-plane crack deflection, which provides a further contribution to toughening.[10] Using 2090-T8E41 as a model material, we now examine these mechanisms in greater detail.

*Plane-strain conditions, as per ASTM E 399 recommendations, are assumed for specimen thicknesses (B) in excess of 2.5 $(K_{Ic}/\sigma_y)^2$, where σ_y is the yield strength.

A. *Crack-Arrester Orientations*

For the T-S (crack-arrester) orientation, an estimate of the toughness increase, compared to the L-T value, can be made by evaluating the effect of crack deflection perpendicular to the crack plane (*e.g.*, shown in Figure 10). Following the linear-elastic solutions of Cotterell and

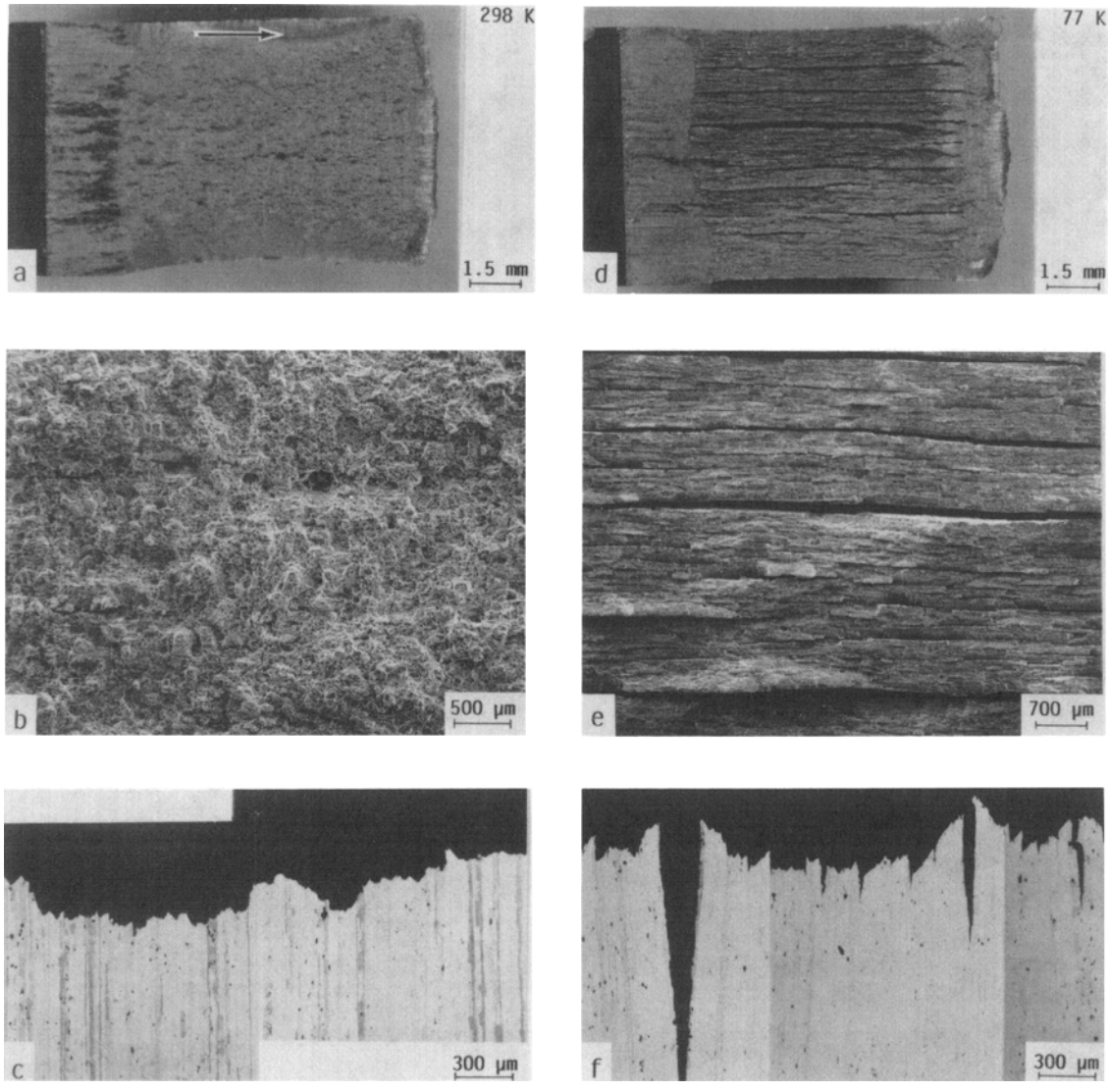

Fig. 6- -Fractography and crack-path morphology for the L-T (crack-divider) orientation, typical of alloys which show a fracture-mode transition between ambient and liquid-nitrogen temperatures (2091-T8X, 8090-T351, 8091-T351), showing ductile microvoid coalescence at 298 K ((*a*), (*b*), and (*c*)) and transgranular shear fracture at 77 K ((*d*), (*e*), and (*f*)). Note the presence of intergranular (short-transverse) delaminations at 77 K. Fracture surfaces are for 2091-T8X. Arrow indicates general direction of crack growth.

Rice[39] for the in-plane deflection (tilt) of a crack through angle θ (deflected segment small compared to crack length), the *local* Mode I and Mode II stress-intensity factors, k_1 and k_2, are given in terms of their *global* values, K_I and K_{II}, and angular functions $a_{ij}(\theta)$ as

$$k_1 = a_{11}(\theta) K_I + a_{12}(\theta) K_{II}$$

$$k_2 = a_{21}(\theta) K_I + a_{22}(\theta) K_{II} \quad [3]$$

Since K_{II} is zero and first-order solutions for $a_{ij}(\theta)$ give

$$a_{11}(\theta) = \cos^3(\theta/2)$$

$$a_{21}(\theta) = \sin(\theta/2)\cos^2(\theta/2) \quad [4]$$

such that the effective stress intensity ahead of a crack deflected through 90 deg is approximately

$$K_{\text{eff}} \approx (k_1^2 + k_2^2)^{1/2} = 0.49 K_I \quad [5]$$

Nonlinear-elastic solutions would suggest a slightly larger effect.[40] Such simple modeling predicts that the toughness in the crack-arrester orientation should be elevated by a factor of roughly two (1/0.49). In 2090-T8E41, the room-temperature L-T toughness is 36 MPa$\sqrt{\text{m}}$; the calculated K_{I_c} value for the T-S orientation is thus of the order of 70 MPa$\sqrt{\text{m}}$, which is close to the measured value of 65 MPa$\sqrt{\text{m}}$.

B. *Crack-Divider Orientations*

To model simply the magnitude of "delamination toughening" for the crack-divider (L-T) orientations, it is assumed that the material behaves like a laminate, where each of m ligaments, separated by the through-thickness splitting, sees a constant tensile stress. At failure, each ligament carries a load P, given in terms of the full specimen width W and thickness B, by

$$P = (K_c^L B W^{1/2})/\{m f(a/W)\} \quad [6]$$

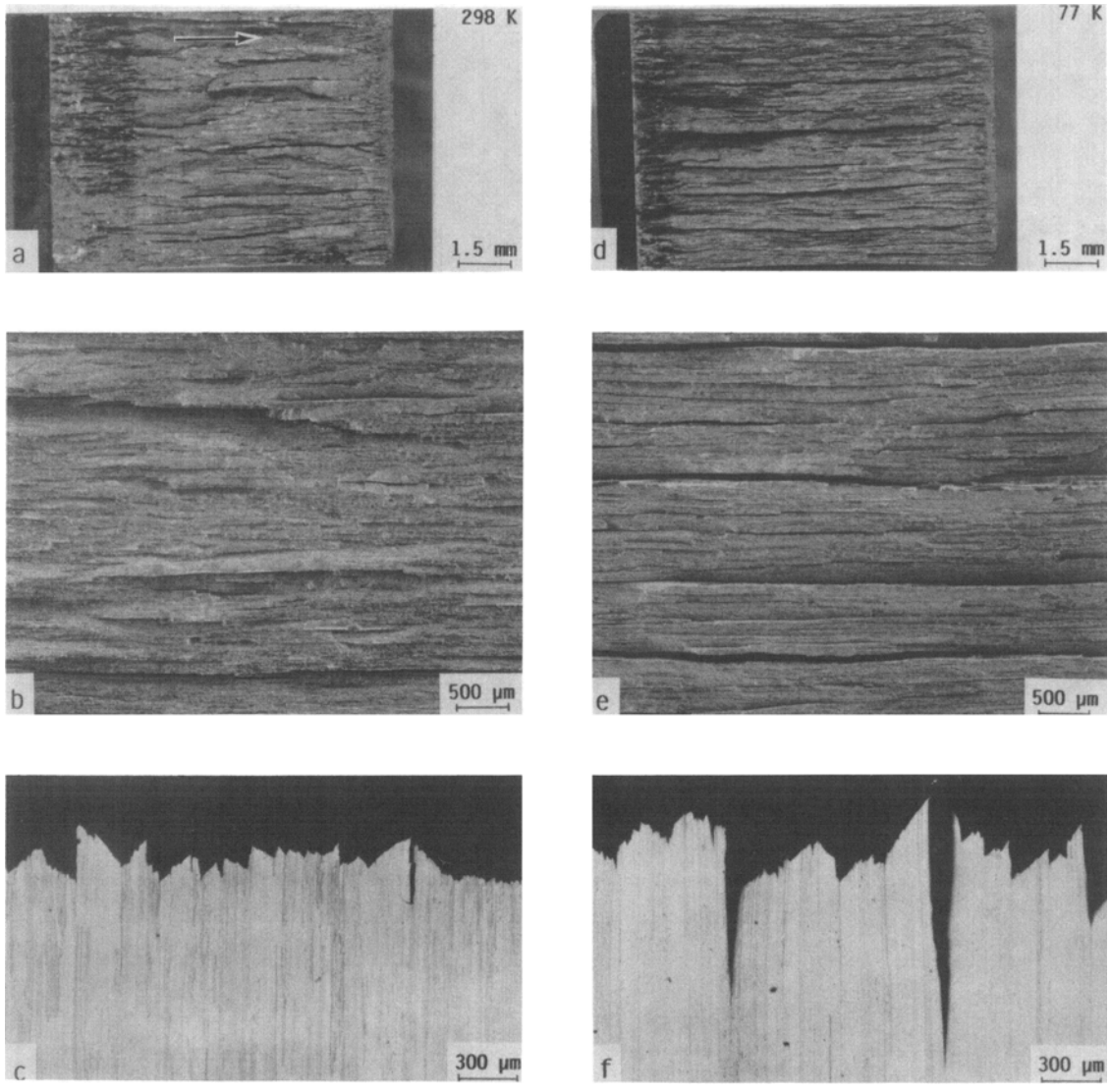

Fig. 7—Fractography and crack-path morphology for the L-T (crack-divider) orientation, typical of alloys which show no fracture-mode transition between ambient and liquid-nitrogen temperatures (2090-T8E41, 2091-T351, 8090-T8X, 8091-T8X), showing transgranular shear fracture at 298 K ((*a*), (*b*), and (*c*)) and 77 K ((*d*), (*e*), and (*f*)). Note how the degree of intergranular (short-transverse) delamination is enhanced significantly at liquid-nitrogen temperatures. Fracture surfaces are for 2090-T8E41. Arrow indicates general direction of crack growth.

where $f(a/W)$ is a function of the crack length-to-width ratio for the specific $C(T)$ specimen geometry[42] and K_c^L is the fracture toughness of a section of thickness B/m. Since the total load carried by the full thickness is mP, the fracture toughness of the laminate will be K_c^L. This constitutes a lower-bound estimate as it assumes no short-transverse strength.

To evaluate this approach in the 2090-T8E41 alloy, fracture-toughness tests were performed at room temperature on 500 μm to 13 mm thick specimens to assess the influence of thickness of K_c; results are shown in Figure 11. It is apparent that the plane-strain toughness value (for thicknesses greater than ~5 to 10 mm) of 36 MPa$\sqrt{\text{m}}$ is increased progressively with decreasing test-piece thickness to a plane-stress value of approximately 45 MPa$\sqrt{\text{m}}$ at a 500 μm thickness, concurrent with the loss in constraint (triaxiality) ahead of the crack tip.

Applying these results to crack-divider (L-T) fractures in 2090 (Figure 7), it is seen that the mean spacing (thickness) of the ligaments between the major through-thickness splits at 298 K is approximately 3 mm; the K_c value at this thickness approaches that of plane strain, *i.e.*, of the order of 36 MPa$\sqrt{\text{m}}$. In contrast, due to enhanced short-transverse delamination, the mean spacing of the split ligaments at 77 K is less than 1 mm; the appropriate K_c for each ligament now is closer to the plane-stress value, *i.e.*, of the order of 45 MPa$\sqrt{\text{m}}$. Using these data, the fracture toughness of 2090 at 77 K would be predicted to be approximately 45 MPa$\sqrt{\text{m}}$ on the basis of the observed delamination, an estimate which is reasonably close to the measured value of 51 MPa$\sqrt{\text{m}}$.

Alternatively, an estimate of the toughness at 77 K can be made from the plane-strain K_{Ic} value at 298 K through prediction of the plane-stress fracture toughness K_c^L relevant to the split-ligament size, using empirical models of Bluhm and others.[42,43,44] Based on assumptions regarding shear-lip (plane-stress) and flat

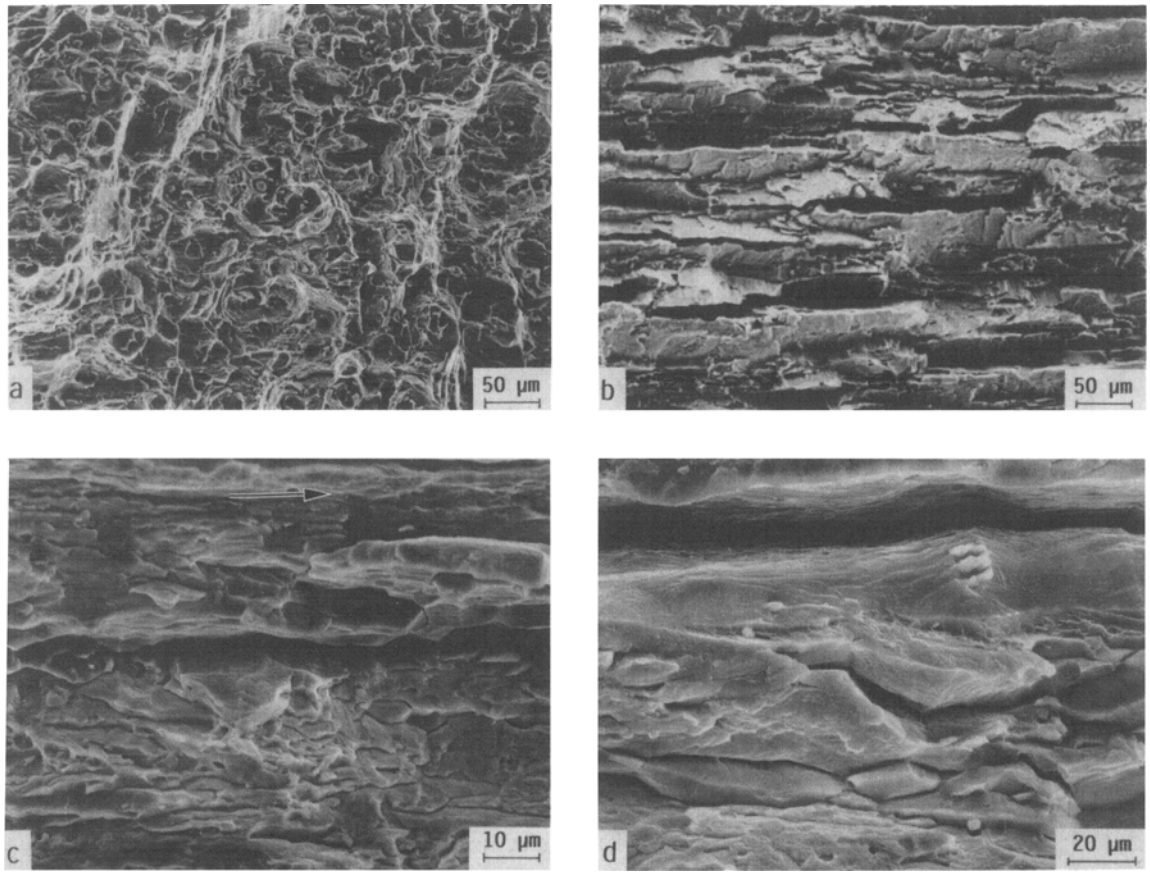

Fig. 8—High magnification scanning electron micrographs of the overload fracture surfaces of 2091-T8X ((*a*) and (*b*)) and 2090-T8E41 ((*c*) and (*d*)) at ambient and liquid-nitrogen temperatures. Note in (a) and (b) the change in failure mode from ductile void coalescence to brittle transgranular shear (interdispersed with intergranular, short-transverse cracking), typical of alloys that show lower toughness at lower temperatures, whereas (in (c) and (d)) alloys that show improved toughness at 77 K show no such transition; failure mode remains predominantly transgranular shear with brittle, intergranular cracking. Horizontal arrow indicates general direction of crack growth.

(plane-strain) fractures being predominantly volumetric and surface phenomena, respectively, and on the dimensions of the plastic-zone size ahead of the crack tip, an expression for K_c^L can be derived as[45]

$$\frac{K_c^L}{K_{Ic}} = \sqrt{1 + \frac{\bar{\varepsilon}_f E}{24\sigma_y}\frac{B_0}{B}} \qquad [7]$$

where σ_y and E refer to the yield strength and elastic modulus, respectively, and $\bar{\varepsilon}_f$ is the true fracture strain appropriate to plane stress conditions (as estimated by the value under uniaxial tension). B is the thickness of the laminate, and B_0 is the maximum thickness in which plane-stress (shear-lip) fracture can develop fully. For the alloy 2090-T8E41, where K_{Ic} at 298 K is 36 MPa$\sqrt{\text{m}}$, σ_y = 552 MPa, $\bar{\varepsilon}_f$ = 0.104, E = 78.3 GPa, and the transition from fully slant to flat fracture occurs at ~2 mm (obtained by metallographically sectioning fractured test pieces of varying thickness), the model predicts values for K_c^L (B = 1 mm), and hence the fracture toughness at 77 K, to be 54 MPa$\sqrt{\text{m}}$, in excellent agreement (albeit fortuitously) with the measured value.

As K_c tends to zero as B tends to zero (Figure 11), it should be noted that, if the short-transverse splitting becomes too extensive, the thickness of the resulting ligaments may become so small (*e.g.*, ~100 μm) that the benefits of delamination (crack-divider) toughening may be compromised. This appears to be the case for overaged 2090, where copious grain and subgrain boundary precipitation and the formation of δ′-precipitate-free-zones[23] increases the tendency for delamination, such that the elevation in fracture toughness at 77 K is far smaller (≲10 pct) than for the T8 condition.

However, both crack-arrester and crack-divider delamination toughening mechanisms are effective only for enhancing the crack-initiation K_{Ic} toughness (as opposed to the crack-growth resistance curve or tearing modulus toughness) if the crack deflection or delamination occurs prior to, or at the point of, crack initiation.* For the present alloys in the peak-aged condition, where little or no stable crack growth appears to precede this instability, deflection and delamination are seen at crack initiation. This is shown for crack-arrester toughening in Figure 10, where splitting along the weak short-transverse planes occurs at the tip of the precrack, and for crack-divider toughening in Figure 12, where the through-thickness delaminations are seen fractographically

*ASTM E 399 specifications for valid K_{Ic} measurements, however, do allow for crack growth of up to approximately 2 pct of the remaining uncracked ligament for defining crack initiation.

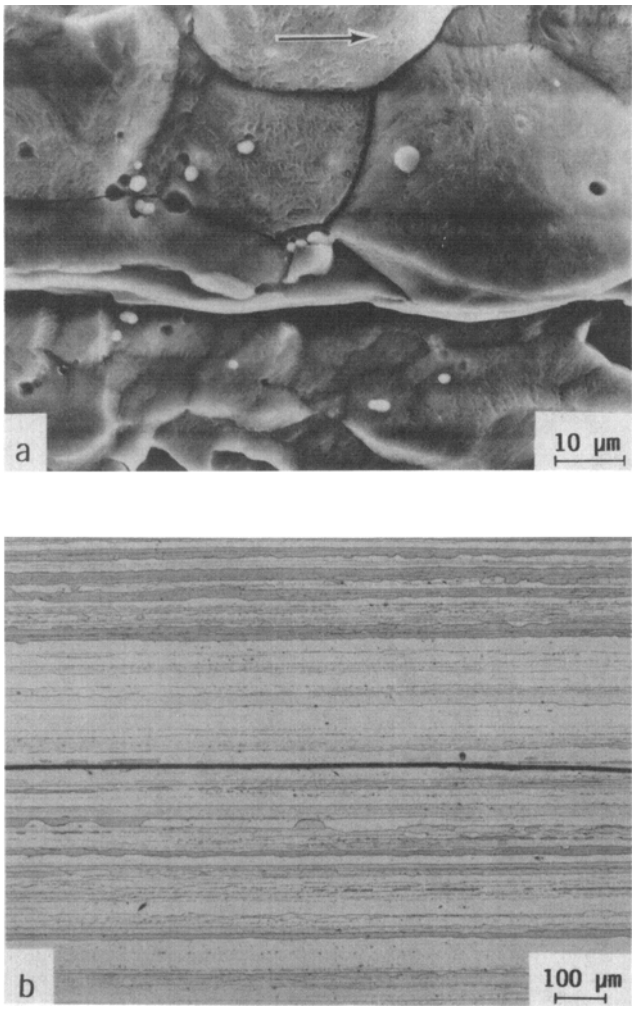

Fig. 9—(*a*) Fractography and (*b*) crack-path morphology for the S-L (crack-delamination) orientation, typical of all alloys at both 77 K and 298 K, showing intergranular delamination-type failure. Fracture surfaces are for 2090-T8E41 and show evidence of ~1 to 2-μm-sized iron- and copper-rich intermetallic particles. Arrow indicates general direction of crack growth.

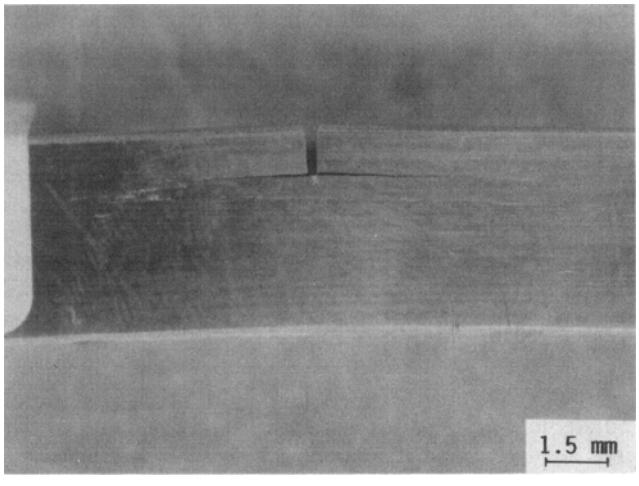

Fig. 10—Delamination toughening in the crack-arrester configuration due to crack deflection at the initiation of crack growth, along weak short-transverse planes in aluminum-lithium alloy 2090-T8E41. Macrograph obtained for the T-S orientation with a measured toughness value of 65 MPa$\sqrt{m}$.

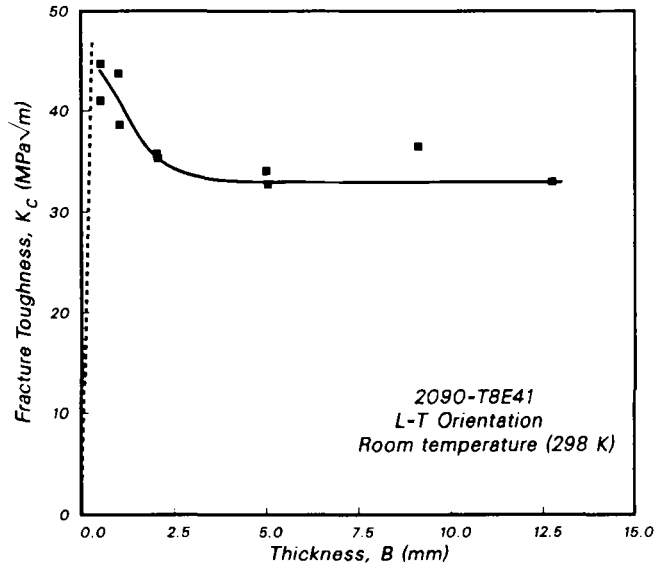

Fig. 11—Variation in Mode I fracture toughness K_c with test-piece thickness B for 2090-T8E41 alloy in the L-T orientation at 298 K. Tests were performed on $C(T)$ specimens, machined from the plate mid-thickness, using anti-buckling restraints to prevent out-of-plane sliding.

immediately at the boundary between the precrack and overload fracture. Moreover, consistent with the arguments of Ritchie and Thompson[46] for nonstationary cracks, both mechanisms are expected to be more potent for improving the crack-growth toughness due to the nature of the nonstationary crack-tip field.[47]

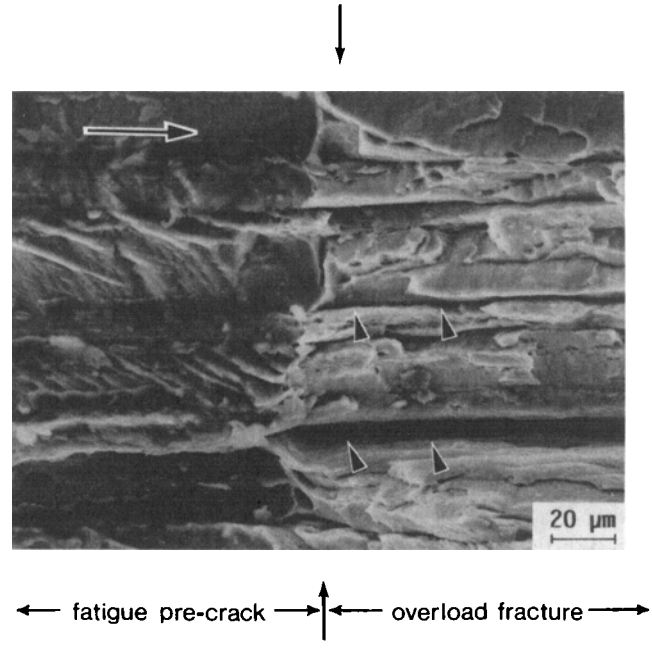

Fig. 12—Scanning electron micrograph in alloy 2090-T8E41 of the boundary (marked by the vertical arrows) between the fatigue precrack region and unstable crack growth due to overload fracture (during K_{Ic} testing), for the crack-divider (L-T) orientation. Note the incidence of short-transverse delaminations (marked by inclined arrows) immediately after the boundary, at crack initiation. Horizontal arrow represents the general direction of crack growth.

C. *Tensile-Ductility Properties*

Further evidence that delamination toughening is primarily responsible for the enhanced cryogenic toughness of certain aluminum-lithium alloys can be gained by examining the tensile-ductility properties. In fact, the observed improvement in uniaxial ductility at low temperatures also appears to be associated with loss of through-thickness constraint. Shown in Figure 13 are fractographs of failed tensile specimens in the 2090-T8E41 alloy, where the increase in ductility from 298 to 77 K is over 25 pct. Extensive short-transverse splitting again is evident at 77 K, but not at 298 K.

However, when the ductility in 2090 is measured under conditions approaching full triaxial (plane-strain) constraint, *i.e.*, at $\sigma/\bar{\sigma} \rightarrow 2$ using circumferentially-notched tensile specimens, no such splitting is observed before crack initiation and the ductility (equivalent fracture strain) now *decreases* (by ~40 pct) with decreasing temperature from 298 to 77 K (Figure 14). It is also apparent that the ductility is reduced by almost an order of magnitude by increasing the triaxial stress-state from that of uniaxial tension($\sigma/\bar{\sigma} = 0.3$) to that approaching plane strain, a result consistent with the observed elevation in fracture toughness in thin sections (Figure 11).

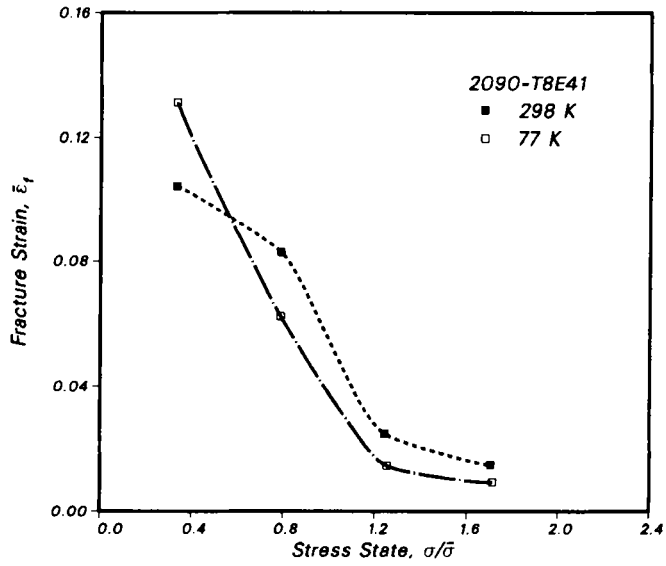

Fig. 14—Influence of stress-state ($\sigma/\bar{\sigma}$) on tensile ductility (equivalent fracture strain, $\bar{\varepsilon}_f$) for 2090-T8E41 (longitudinal orientation) at 298 K and 77 K. Note the *decrease* in plane-strain ductility and *increase* in uniaxial ductility with decrease in temperature.

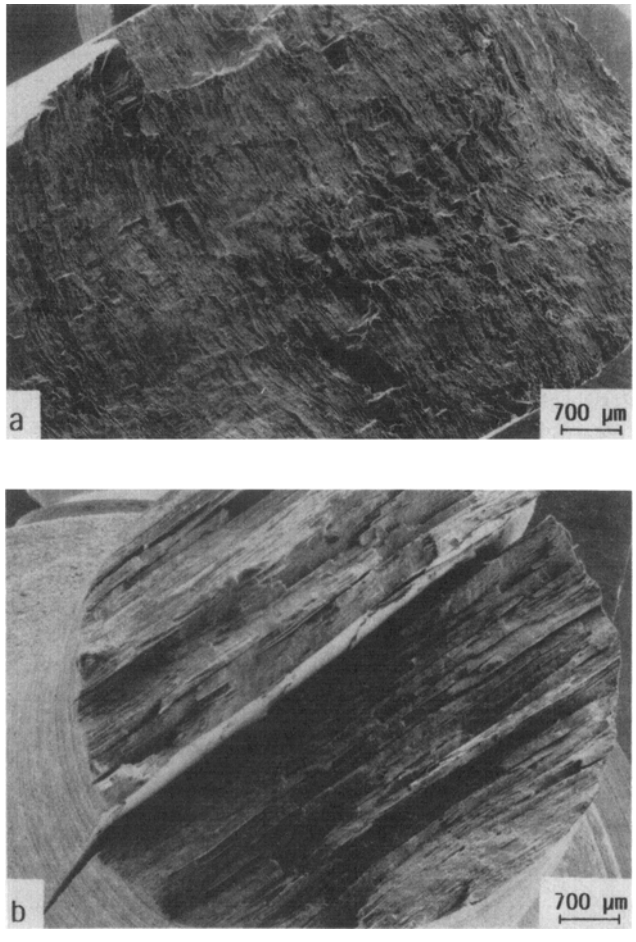

Fig. 13—Scanning electron micrographs of the fracture surfaces of unnotched round tensile specimens of 2090-T8E41 (longitudinal orientation), tested at (*a*) 298 K and (*b*) 77 K, showing the presence of extensive short-transverse delamination at liquid-nitrogen temperatures.

D. *Microstructural Effects*

Finally, the salient microstructural factors in aluminum-lithium alloys, which include the degree of slip planarity, nature of matrix and grain-boundary precipitation, size of precipitate-free-zones (PFZs), and extent of anisotropy can have a dual effect on fracture toughness. First, marked planarity of slip generally is regarded as intrinsically detrimental to the toughness of ductile alloys as it promotes earlier linkage of microvoids, yet in Al-Li alloys it may be beneficial extrinsically as it also promotes crack deflection and bifurcation.[48] Second, extensive grain-boundary precipitation and attendant PFZs similarly can be detrimental to toughness by promoting intergranular fracture,[49] especially in planar-slip materials, yet such precipitation also can promote short-transverse splitting, thereby improving the low-temperature toughness. The latter behavior is best shown by 8091-T8X, which exhibits widespread grain-boundary precipitation, ~1-μm-wide lithium-depleted δ'-PFZs,[12] and correspondingly very low toughness (both L-T and S-L) at 298 K. However, at 77 K, the associated increase in short-transverse splitting results in a 90 pct increase in L-T toughness. Finally, anisotropy in the form of planes of weakness parallel to the rolling plane clearly is detrimental to short-transverse properties, yet this provides the major contribution to crack-divider and crack-arrester delamination toughening. The peak-aged 2090-T8E41 alloy with its strong deformation texture is perhaps the best example of this; apart from 8091-T8X, its short-transverse toughness properties are among the worst, yet, in the L-T orientation, it shows the highest overall toughness over the temperature range from liquid nitrogen to ambient. In fact, in spite of limited short-transverse properties, 2090-T8E41 appears to exhibit an optimal combination of intrinsic properties (homogeneous matrix precipitation, no grain-boundary

precipitation or PFZs) and extrinsic properties (crack-divider and crack-arrester delamination toughening), which result in the best combination of strength and toughness properties among commercial aluminum-lithium alloys.

V. CONCLUSIONS

Based on a study of the fracture-toughness and tensile behavior of commercial aluminum-lithium alloys, 2090-T8E41, 2091-T351, 2091-T8X, 8090-T351, 8090-T8X, 8091-T351, and 8091-T8X, at ambient (298 K) and cryogenic (77 K) temperatures, the following conclusions may be drawn:

1. In all commercial alloys at both 298 and 77 K, the fracture toughness measured in the L-T (crack-divider) orientation was significantly higher (by 18 to 375 pct) than in the S-L (crack-delamination) orientation. Toughness values measured at 298 K in 2090-T8E41 for the T-S (crack-arrester) orientation were 80 pct larger than the L-T value and 276 pct larger than the S-L value.
2. All commercial alloys displayed increases in strength, uniaxial tensile-ductility, and strain-hardening rates with decrease in temperature from 298 to 77 K.
3. Improvements in the plane-strain fracture toughness at cryogenic temperatures, however, are not typical of all commercial alloys. While alloys 2090-T8E41, 2090-T351, 8090-T8X, and 8091-T8X showed such an *increase* in K_{Ic} for the L-T orientation between 298 and 77 K, alloys 2091-T8X, 8090-T351, and 8091-T351 conversely showed a corresponding *decrease*. The toughness of all alloys decreased with *decrease* in temperature for the S-L orientation.
4. The reduction in fracture toughness (L-T orientation) with decrease in temperature, shown by alloys 2091-T8X, 8090-T351, and 8091-T351, was concurrent with a fracture-mode transition from ductile void coalescence at 298 K to a transgranular shear fracture (with some evidence of short-transverse delamination) at 77 K.
5. The increase in fracture toughness (L-T orientation) with decrease in temperature, shown by alloys 2090-T8E41, 2091-T351, 8090-T8X, and 8091-T8X, conversely was associated with no (macroscopic) fracture-mode transition; however, the degree of intergranular, short-transverse delamination (splitting) on the fracture surface was enhanced significantly at 77 K, consistent with the observed decrease in S-L toughness.
6. Analogous to the behavior of laminated materials, the increase in L-T toughness, shown by alloys 2090-T8E41, 2091-T351, 8090-T8X, and 8091-T8X with decrease in temperature, is ascribed primarily to a mechanism of crack-divider delamination toughening. Essentially, the increased incidence of through-thickness (short-transverse) splitting at low temperature results in a loss of through-thickness constraint, causing the plane-strain fracture process to be divided into several parallel (thin-sheet) plane-stress fractures with higher K_c values. Thin-sheet (plane-stress) K_c values in 2090-T8E41 were found to be consistent with the observed increase in toughness.
7. Similarly, the very high toughness values measured in 2090-T8E41 for the T-S orientation are ascribed to crack-arrester delamination toughening, where short-transverse splitting now causes a decrease in *local* stress intensity at the crack tip from crack deflection or bifurcation (through approximately 90 deg).
8. The observed *increase* in uniaxial tensile ductility (L orientation) with decrease in temperature also appeared to be associated with loss of constraint from enhanced short-transverse delamination at 77 K. Tensile ductility values measured in 2090-T8E41 under more constrained conditions approaching plane strain, accordingly, were found to *decrease* at lower temperatures.
9. Despite low short-transverse toughness, optimal strength/toughness (longitudinal) properties were found at both 298 and 77 K in the 2090-T8E41 alloy. Such behavior is attributed primarily to the anisotropic, unrecrystallized, and highly elongated grain structure (with homogeneous matrix precipitation) in peak-aged 2090, which leads to poor short-transverse toughness but promotes crack-divider and crack-arrester delamination toughening, especially at cryogenic temperatures, in the perpendicular orientations.

ACKNOWLEDGMENTS

This work was supported by the Director, Office of Energy Research, Office of Basic Energy Sciences, Materials Sciences Division of the United States Department of Energy through Contract No. DE-AC03-76SF00098. Alloys were supplied by Alcoa, Boeing, Northrop, and AFWAL (the latter through the NAVAIR Collaborative Test Program). Thanks are due to Drs. Bretz, Bucci, Chanani, Petrak, Quist, Sawtell, and Scarich for their advice and help in procuring materials, to Professor J.W. Morris and J. Glazer for helpful discussions, to J.E. Miles and L. Gill for experimental assistance, and to the journal referees for their constructive suggestions.

REFERENCES

1. J. Glazer, S.L. Verzasconi, E.N. Dalder, W. Yu, R.A. Emigh, R.O. Ritchie, and J.W. Morris: *Adv. Cryo. Eng.*, 1986, vol. 32, pp. 397-404.
2. D. Webster: *Metals Progress*, 1984, vol. 125, pp. 31-37.
3. D. Webster: in *Aluminum-Lithium Alloys III*, C. Baker, P.J. Gregson, S.J. Harris, and C.J. Peel, eds., Institute of Metals, London, U.K., 1986, pp. 602-09.
4. R.C. Dorward: *Scripta Metall.*, 1986, vol. 20, pp. 1379-83.
5. D. Dew-Hughes, E. Creed, and W.S. Miller: *Mater. Sci. Tech.*, 1988, vol. 4, pp. 106-12.
6. F.G. Nelson and J.G. Kaufman: in *Fracture Toughness Testing at Cryogenic Temperatures*, ASTM STP 496, American Society for Testing and Materials, Philadelphia, PA, 1971, pp. 27-39.
7. J. Glazer, S.L. Verzasconi, R.R. Sawtell, and J.W. Morris: *Metall. Trans. A*, 1987, vol. 18A, pp. 1695-701.
8. F.A. Johnson and J.C. Radon: *Int. J. Fracture*, 1972, vol. 8, pp. 21-36.
9. D. Webster: *Metall. Trans. A*, 1987, vol. 18A, pp. 2181-93.
10. K.T. Venkateswara Rao, H.F. Hayashigatani, W. Yu, and R.O. Ritchie: *Scripta Metall.*, 1988, vol. 22, pp. 93-98.

11. C.M. Carman, D.F. Armiento, and H. Markus: in *ICF-1*, Proc. of 1st Intl. Conf. on Fracture, T. Yokobori, T. Kawasaki, and J.L. Swedlow, eds., Sendai, Japan, 1965, vol. 1, pp. 995-1038.
12. K.T. Venkateswara Rao and R.O. Ritchie: *Mater. Sci. Tech.*, 1989, vol. 5, in press.
13. H.M. Flower and P.J. Gregson: *Mater. Sci. Tech.*, 1987, vol. 3, pp. 81-90.
14. P. Meyer and B. Dubost: in *Aluminum-Lithium Alloys III*, C. Baker, P.J. Gregson, S.J. Harris, and C.J. Peel, eds., Institute of Metals, London, U.K., 1986, pp. 37-46.
15. M.H. Tosten, A.K. Vasudévan, and P.R. Howell: *Metall. Trans. A*, 1988, vol. 19A, pp. 51-66.
16. K.V. Jata and E.A. Starke: *Metall. Trans. A*, 1986, vol. 17A, pp. 1011-26.
17. A.K. Vasudévan, W.G. Fricke, R.C. Malcolm, R.J. Bucci, M.A. Przystupa, and F. Barlat: *Metall. Trans. A*, 1988, vol. 19A, pp. 731-32.
18. J. Hirsch, O. Engler, K. Lücke, M. Peters, and K. Welpmann: *J. Physique Coll.*, 1987, vol. C3, pp. 605-11.
19. G.R. Yoder, P.S. Pao, M.A. Imam, and L.A. Cooley: *Scripta Metall.*, 1988, vol. 22, pp. 1241-44.
20. R.O. Ritchie, W.L. Server, and R.A. Wullaert: *Metall. Trans. A*, 1978, vol. 10A, pp. 1557-70.
21. P.W. Bridgman: *Studies in Large Flow and Fracture*, McGraw-Hill, New York, NY, 1952.
22. R.J. Bucci: *Eng. Fract. Mech.*, 1979, vol. 12, pp. 407-41.
23. K.T. Venkateswara Rao and R.O. Ritchie: *Mater. Sci. Eng.*, 1988, vol. 100, pp. 23-30.
24. D.E. Pettit and J.M. Van Orden: in *Fracture Mechanics*, ASTM STP 677, American Society for Testing Materials, Philadelphia, PA, 1979, pp. 106-24.
25. W.S. Miller, M.P. Thomas, D.J. Lloyd, and D. Creber: in *Aluminum-Lithium Alloys III*, C. Baker, P.J. Gregson, S.J. Harris, and C.J. Peel, eds., Institute of Metals, London, U.K., 1986, pp. 584-93.
26. R.O. Ritchie, L.C.E. Geniets, and J.F. Knott: in *Microstructure and Design of Alloys* (Proc. ICMSA-3), Institute of Metals/Iron and Steel Institute, London, U.K., 1973, vol. 1, pp. 124-28.
27. H.L. Leichter: *J. Spacecraft*, 1966, vol. 3, pp. 1113-20.
28. J.D. Embury, N.J. Petch, A.E. Wraith, and E.S. Wright: *Trans. TMS-AIME*, 1967, vol. 239, pp. 114-18.
29. J.G. Kaufman: *J. Basic Eng.*, Trans. ASME, Series D, 1967, vol. 89, pp. 503-07.
30. N.G. Ohlson: *Eng. Fract. Mech.*, 1974, vol. 6, pp. 459-72.
31. S.D. Antolovich, K. Kasi, and G.R. Chanani: in *Fracture Toughness*, ASTM STP 514, American Society for Testing Materials, Philadelphia, PA, 1972, pp. 135-50.
32. S. Floreen, H.W. Hayden, and J.Q. Steigelman: *Trans. ASM*, 1969, vol. 62, pp. 812-15.
33. R.A. Schmidt and T.J. Lutz: in *Fracture Mechanics Applied to Brittle Materials*, ASTM STP 678, American Society for Testing Materials, Philadelphia, PA, 1979, pp. 166-82.
34. M. Sakai, R.C. Bradt, and D.B. Fischbach: *J. Mater. Sci.*, 1986, vol. 21, pp. 1491-501.
35. G.E. Pellissier: *Eng. Fract. Mech.*, 1968, vol. 1, pp. 55-75.
36. R.J. Stokes and C.H. Li: *Trans. TMS-AIME*, 1964, vol. 230, pp. 1104-10.
37. K. Markström: *Eng. Fract. Mech.*, 1972, vol. 4, pp. 593-603.
38. J. Cook and J.E. Gordon: *Proc. Roy. Soc. A*, 1964, vol. A282, pp. 509-20.
39. B. Cotterell and J.R. Rice: *Int. J. Fract.*, 1980, vol. 16, pp. 155-69.
40. S. Suresh and C.F. Shih: *Int. J. Fract.*, 1986, vol. 30, pp. 237-59.
41. H. Tada, P.C. Paris, and G.R. Irwin: in *The Stress Analysis of Cracks Handbook*, 2nd ed., Paris Prod. Inc. & Del Research Corp., St. Louis, MO, 1985.
42. J.I. Bluhm: *ASTM Proc.*, 1961, vol. 61, pp. 1324-31.
43. D.P. Isherwood and J.G. Williams: *Eng. Fract. Mech.*, 1970, vol. 2, pp. 19-35.
44. G.C. Shih and R.J. Hartranft: *Int. J. Fract.*, 1973, vol. 9, pp. 75-82.
45. D. Broek: *Elementary Engineering Fracture Mechanics*, 3rd ed., Martinus Nijhoff, The Hague, The Netherlands, 1984.
46. R.O. Ritchie and A.W. Thompson: *Metall. Trans. A*, 1985, vol. 16A, pp. 233-48.
47. W.J. Drugan, J.R. Rice, and T.-L. Sham: *J. Mech. Phys. Solids*, 1982, vol. 30, pp. 447-73.
48. S. Suresh, A.K. Vasudévan, M. Tosten, and P.R. Howell: *Acta Metall.*, 1987, vol. 35, pp. 25-46.
49. A.K. Vasudévan and R.D. Doherty: *Acta Metall.*, 1987, vol. 35, pp. 1193-219.